Investigation of Aquifer-Estuary Interaction Using Wavelet Analysis of Fiber-Optic Temperature Data

by R.D. Henderson,[1,2] F.D. Day-Lewis[1,*], C.F. Harvey[3]

[1]*U.S.Geological Survey, Office of Ground Water, Branch of Geophysics, 11 Sherman Place, Unit-5015, Storrs CT 06269*

[2]*Center for Integrative Geosciences, Beach Hall, Unit-2045, U. Connecticut, Storrs CT 06269*

[3]*Dept. of Civil & Environmental Engineering, MIT, 77 Massachusetts Ave., Cambridge MA 02139*

[*]Corresponding Author:
daylewis@usgs.gov
860.487.7402 x21

Abstract

Fiber-optic distributed temperature sensing (FODTS) provides sub-minute temporal and meter-scale spatial resolution over kilometer-long cables. Compared to conventional thermistor or thermocouple-based technologies, which measure temperature at discrete (and commonly sparse) locations, FODTS offers nearly continuous spatial coverage, thus providing hydrologic information at spatiotemporal scales previously impossible. Large and information-rich FODTS datasets, however, pose challenges for data exploration and analysis. To date, FODTS analyses have focused on time-series variance as the means to discriminate between hydrologic phenomena. Here, we demonstrate the continuous wavelet transform (CWT) and cross-wavelet transform (XWT) to analyze FODTS in the context of related hydrologic time series. We apply the CWT and XWT to data from Waquoit Bay, Massachusetts to identify the location and timing of tidal pumping of submarine groundwater.

Final copy as submitted to Geophysical Research Letters for publication as: Henderson, R.D., Day-Lewis, F.D., and Harvey, C.F., 2009, Investigation of aquifer-estuary interaction using wavelet analysis of fiber-optic temperature data: Geophysical Research Letters, 36, L06403, doi:10.1029/2008GL036926.

1. Introduction

Temperature data have long been used to investigate groundwater/surface-water interaction (Anderson, 2005). Whereas groundwater temperature is relatively constant, surface-water temperature changes with seasonal, diurnal, and episodic forcing. Changes in temperature therefore form a basis to infer the locations and rates of submarine groundwater discharge (SGD) (Taniguchi et al., 2003). Historically, such work involved point measurements using thermistors or thermocouples, and interpretation based on numerical modeling (e.g., Constantz and Stonestrom, 2003) or time-series analysis (e.g., Hatch et al., 2006). Fiber-optic distributed temperature sensing (FODTS) now provides the means to measure temperature over large areas at much finer spatial and temporal scales than previously practical (Selker et al., 2006). The technology is capable of measuring temperature over multi-kilometer-long cables, with meter-scale spatial and sub-minute temporal resolution, and precision approaching 0.01 °C. Such enormous and complex datasets, however, pose substantial challenges for data exploration and analysis.

To date, analysis of FODTS data has focused on examination of the time series of temperature along a cable to identify zones of relative low and high variability. Low variability is interpreted as the modulating effect of groundwater input (Lowry et al., 2007; Moffet et al., 2008), and high variability is interpreted as the result of solar radiation, air temperature, precipitation, and runoff. In some hydrologic systems, variable groundwater input may, in fact, enhance temperature variability, as in the case of tidal pumping.

In principle, spectral analysis is capable of decomposing a time series into its component frequencies, thus enabling identification of scales of variability (e.g., Kendall and Hyndman, 2007). Traditional spectral analysis is based on the discrete time Fourier transform (DTFT) which assumes that the time series is a linear superposition of periodic components; this

assumption is strictly valid only for stationary time series. In the presence of non-periodic behavior from episodic or extreme events, the DTFT can produce misleading results (e.g., Torrence and Compo, 1998); furthermore, with transformation to the frequency domain, all time localization is lost. Although the DTFT provides broad insight into the processes affecting an entire time series, other approaches are needed to capitalize fully on the information available from FODTS. Here, we propose that wavelet-based approaches are well suited to this purpose.

The continuous wavelet transform (CWT) and cross-wavelet transform (XWT) increasingly are used for analysis of non-stationary signals (e.g., Torrence and Compo, 1998; Kang and Lin, 2007). Compared to approaches based on the DTFT, the CWT allows for the temporal localization of dominant frequency components in the time series; i.e., the timing of onset or cessation of a signal's components. Similarly, the XWT quantifies cross-correlation between non-stationary signals. The capability to resolve changes in frequency content over time is critical to inference of system dynamics and correlation between multiple time series affected by episodic events and different forcing mechanisms (e.g., tidal, diurnal, and seasonal).

2. Methods

We briefly review the FODTS and wavelet methods and then focus on their combined application to investigate SGD.

2.1. FODTS

FODTS has been used to monitor hydrologic processes in fluvial (Selker et al., 2006), salt-marsh (Moffett et al., 2008), glacial (Tyler et al., 2008), and wetland settings (Lowry et al., 2007). In FODTS, laser light is transmitted down a fiber-optic cable and some of the energy is scattered back up the cable by various physical mechanisms. In Raman backscatter, the scatter occurs at frequencies both higher (anti-Stokes) and lower (Stokes) than that of the transmitted

light. The amplitude of the Raman anti-Stokes signal is more sensitive to temperature than that of the Stokes signal, providing the basis for temperature measurement. An FODTS measurement is localized to an interval of cable using optical time-domain reflectometry (OTDR), which is based on a time-of-flight calculation given by the speed of light (Selker et al., 2006). In this work, we use a Lios 2000/4000, which uses optical frequency domain reflectometry (OFDR). (Note that use of trade, product, or firm names is for descriptive purposes only and does not imply endorsement by the U.S. Government.) OFDR is similar in concept to OTDR, except that backscatter is analyzed in the frequency domain.

2.2. Wavelets

Prior to the advent of wavelets, the DTFT was the standard tool to transform a time series, $g[n]$, into the frequency domain:

$$G(\omega) = \sum_{-\infty}^{\infty} g[n] e^{-i\omega n} \quad , \tag{1}$$

where $G(\omega)$ is the transformed signal, ω is frequency, and n is the time. By examination of power, $|G(\omega)|^2$, the signal's frequency content is characterized. Although the DTFT offers insight into periodic features present over an entire signal, the transform cannot characterize when non-stationary behavior occurs. Where phenomena are localized over certain time intervals, the DTFT has limited utility. The CWT is more appropriate to identify, for example, when the tide versus the diurnal heating dominates estuarine thermal dynamics.

In contrast to the DTFT, which decomposes the time series into constituent sinusoids of varying amplitude, the CWT convolves a basis function, or wavelet, with the time-domain signal. A wavelet is a unit-energy signal localized in time and frequency. In the CWT, the wavelet is dilated and scaled to isolate various frequency components temporally. As the wavelet is stretched and downscaled to resolve lower frequency components, it loses temporal

resolution. Conversely, higher frequency features are well resolved in time, but not frequency (Torrence and Compo, 1998); thus, the CWT cannot achieve high resolution in both frequency and time simultaneously.

A number of wavelets have been described (e.g., Morlet, Paul, and derivative-of-Gaussian), each with associated advantages and disadvantages. We use a Morlet wavelet, which is mathematically equivalent to a sinusoid damped by a Gaussian. The Morlet wavelet because it is complex-valued and localized in both time and space, allowing extraction of phase information using the XWT. The Morlet wavelet function, ψ_0, is:

$$\psi_0(\eta) = \pi^{-1/4} e^{i\omega_0\eta} e^{-1/2\eta^2} \quad , \tag{2}$$

where ω_0 is dimensionless frequency and η is dimensionless time, depending on the time scale of the data.

The CWT of a time series is:

$$W_n^X(s) = \sqrt{\frac{\delta t}{s}} \sum_{n'=1}^{N} x_{n'} \psi_0[(n'-n)\frac{\delta t}{s}], \tag{3}$$

where $W_n^X(s)$ is the transformed time series for scale *s*; δt is the time step; *n* is the time; and n' is reversed time. Wavelet power is calculated as $|W_n^X(s)|^2$ and normalized by the signal variance. Edge artifacts develop in CWT because the wavelet is not completely localized in time (Grinsted et al., 2004), and the calculation is performed in frequency space, which commonly requires zero-padding to achieve a time series of length 2^N. A cone of influence is used to delineate the region of possibly spurious results. Statistical significance is tested by comparison of power with the estimated noise spectrum for the time series, commonly assuming red noise (Torrence and Compo, 1998).

The XWT is used to infer coincident high power between two time series by multiplying the real portion of one signal by the complex portion of another:

$$W^{XY} = W^{X} W^{Y*}, \quad (4)$$

where W^{XY} is the XWT between signals X and Y; W^{X} is the real portion of the CWT of X; and W^{Y*} is the complex conjugate of the CWT of Y. XWT power is calculated by $|W^{XY}|^2$. The lag between time series is given by the phase angle between the real and complex portions of the XWT (Grinsted et al., 2004); phase information is the basis for several methods to infer groundwater discharge rates (e.g., Hatch et al., 2006).

3. Field Experiment

The FODTS experiment was conducted in June-July 2007 at Waquoit Bay National Estuarine Research Reserve (WBNERR), East Falmouth, Massachusetts. The bay is approximately 3 km^2, has an average depth of about 1 m, and a contributing watershed area of 56.45 km^2 (Cambareri and Eichner, 1998). Beneath the bay, an approximately 11-m-thick permeable layer overlies less permeable fine sand, silt and clay. Beneath this aquifer, flow is restricted by glacial till and bedrock (Michael et al., 2003). Fresh SGD occurs along a narrow band on the beach and several meters into the bay (Michael et al., 2005).

Tidal fluctuations create head differences between the coastal aquifer and the bay that drive “tidal pumping” (Michael et al., 2005). Tides cycle over a period of 12.33 hours, alternating between greater and lower amplitude. Waquoit Bay has an average tidal range of approximately 0.7 m. In addition, spring and neap tides modulate the tidal amplitude and occur on the 4-week lunar cycle. At spring tides, the tidal range is largest, and the elevated bay level delivers saltwater by run-up and wave action farther onto the beach face. Neap tides have smaller daily ranges, with the amplitude of the larger tide reduced to near that of the smaller tide.

A fiber-optic cable was installed semi-permanently at the WBNERR in October 2006. The FODTS instrument is housed onshore and the cable runs 50-m offshore in a single out-and-

back transect perpendicular to shore. The cable was buried to a depth of approximately 0.5 m near-shore (below the water table under the beach) and allowed to sink into soft sediments offshore. Data were collected from 4 June 2007 to 16 July 2007 in 29-sec intervals with approximately 1-m spatial resolution. During this period, the surface water ranged from approximately 16 to 29 °C, and groundwater remained constant at approximately 11 °C; hence fresh SGD was colder than bay water.

4. Results

The FODTS and meteorological data show tidal and diurnal periodicity, non-stationary episodic variability from storms, and a trend of increasing temperature from seasonal warming (Figure 1). The data also show a prominent cold anomaly between approximately 7-13 m from shore, where Michael et al. (2003, 2005) found a zone of fresh SGD. This zone persists for the duration of the experiment, but close inspection indicates slight cooling at low tides (Figure 1b). Beyond 13 m off-shore, temperature changes are not dominated by tides but rather by diurnal solar heating/cooling (Figure 1c).

Before analyzing transforms of the data, we first consider the temporal variance of the FODTS data (Figure 1d) at different distances from shore. The lowest variance occurs at the foot of the bluff (0 m), where the cable is buried deeper than elsewhere, but also below the level of groundwater on the beach face. Other areas of low variance occur at approximately 9 m (within the SGD zone) and 34 m from shore. Conversely, the boundaries of the SGD zone (7 and 13 m) show higher variance.

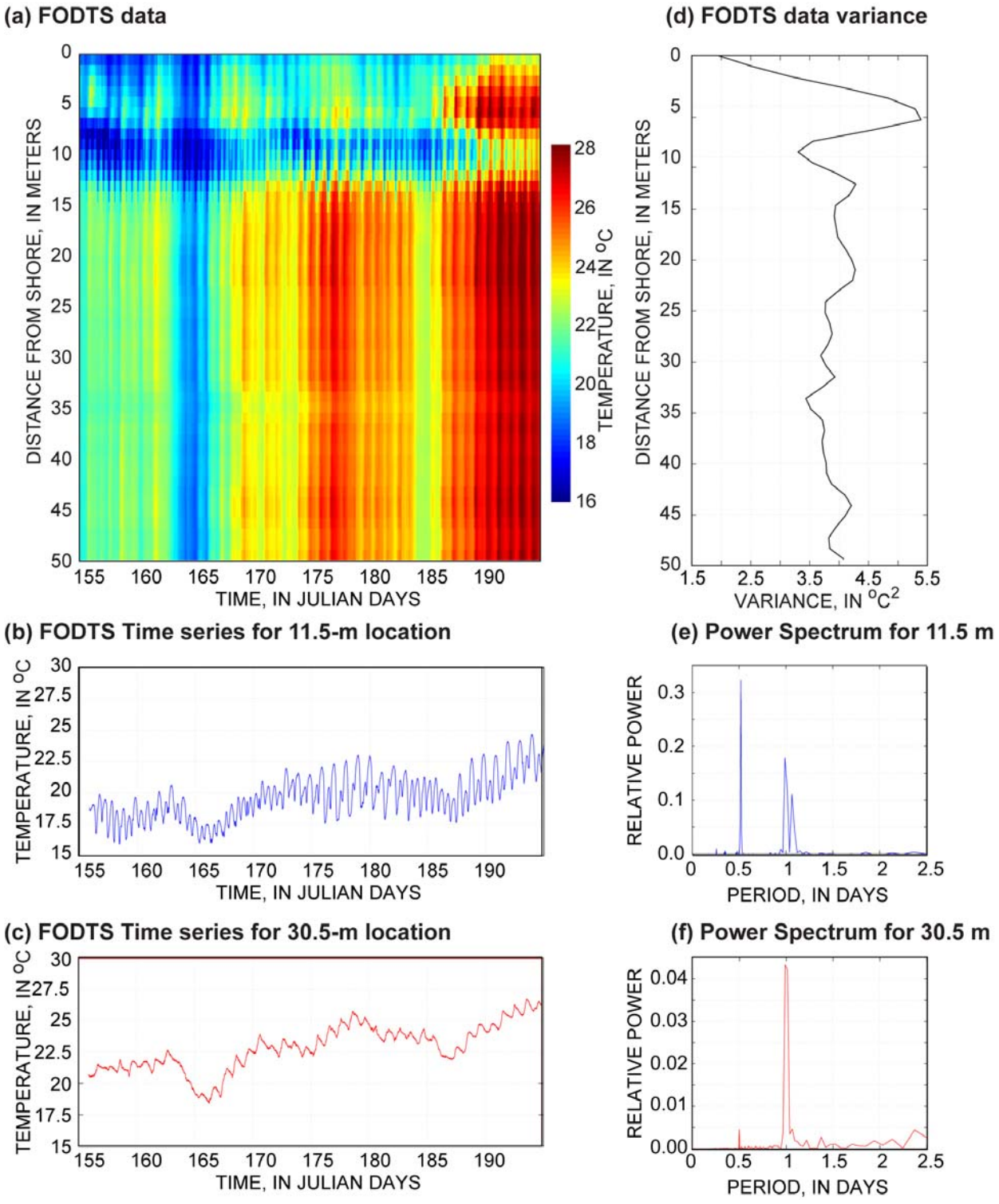

Figure 1. (a) Temperature measured by FODTS; (b) FODTS data for the 11.5-m location; (c) FODTS data for the 30.5-m location; (d) variance of FODTS calculated over all times; (e) power spectrum of FODTS data for the 11.5-m location calculated by DTFT; and (f) power spectrum of FODTS data for the 11.5-m location calculated by DTFT.

Spectral decomposition provides information about periodicities in temperature that cannot be characterized by the variance alone. We analyze the FODTS time series at two locations—the first inside the zone of fresh SGD (11.5 m) and the second beyond it (30.5 m). At 11.5 meters from shore, tidal influences are evident in the time series of temperature (Figure 1b) whereas at 30.5 m from shore, diurnal influences dominate (Figure 1c). These periodicities are confirmed by the power spectra calculated from the DTFT (Equation 1), which show dominant periods of 0.5 day and 1 day for the 11.5-m FODTS data (Figure 1e), and a dominant period of 1 day at 30.5 m from shore (Figure 1f).

Our results demonstrate that DTFT provides a useful characterization of periodic behavior in the temperature data where this behavior is stationary for the duration of the sampling; however, both time series (Figures 1b and 1c) extracted from our data clearly show temporal patterns that are not captured by the DTFT transform. Both series show changes in temperature that are not periodic within the duration of the experiment, and, particularly at the 11.5-m location, there are obvious shifts in the amplitude of the periodic temperature changes.

In contrast to the DTFT, the CWT provides information about non-stationary temperature variations. Wavelet power for a given time and period is plotted and normalized by the time-series variance at the two locations considered above (Figure 2a). At 11.5 m, statistically significant power is observed at the 0.5-day, 1-day, and 0.25-day periods. The 0.5-day period is dominant and always present, indicating the effect of tidal pumping at this location. The 1-day period also is present, but fades between Julian Days (JD) 169-172 and 186-187. At 30.5 m, high power is present at the 1-day period but fades between JDs 163-165.

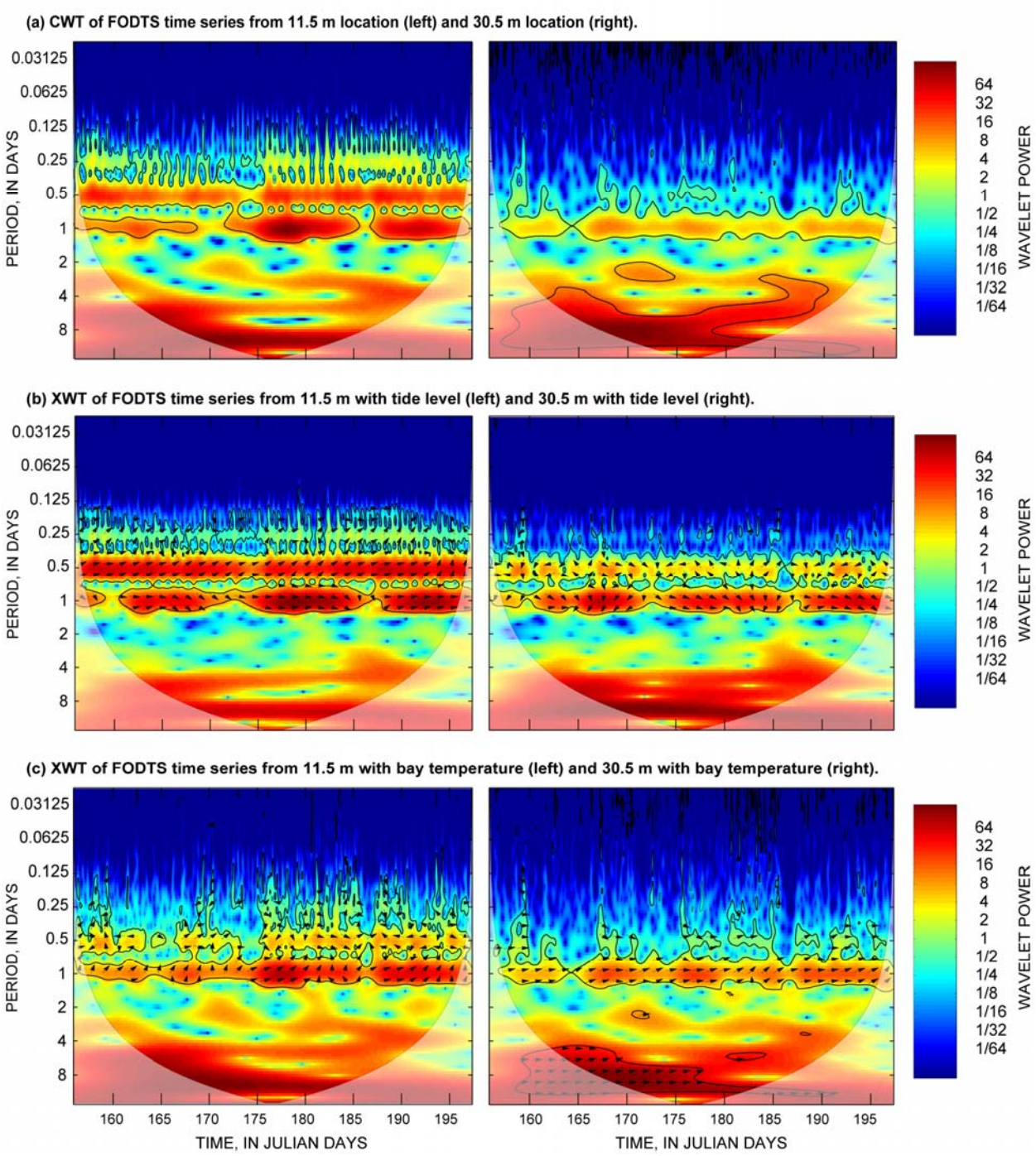

Figure 2. (a) Continuous wavelet transform of FODTS data from the 11.5-m and 30.5-m locations; (b) XWT of the FODTS data from the 11.5-m and 30.5-m locations with tide level; and (c) XWT of the FODTS data from the 11.5-m and 30.5-m locations with bay temperature.

We analyze the XWT between FODTS temperature and tide level and then bay temperature. In instances of statistically significant, correlated power, the phase lag between two time series at a given location is plotted as an arrow (Figures 2b, 2c). Arrows point right for time series in-phase and left for out-of-phase. Vertical arrows indicate that time series are 90 degrees out-of-phase, with arrows pointing up when X leads Y (as defined in Equation 4) and down when Y leads X. At 11.5 m, the XWT with tide (Figure 2b) displays high power at 0.5-day, 1-day and 0.25-day periods. The calculated phase lag indicates the two time series are phase locked in the 0.5-day period with tidal fluctuations leading temperature fluctuations by 3.4 hours. At 30.5 m, the XWT with tide (Figure 2b) exhibits high power at the 1-day and 0.5-day periods, but with highly variable phase lags indicating that the signals have high coincident power (where the amplitudes are both correlated) but are decoupled.

Bay temperature changes diurnally with solar heating of the estuary floor. We apply the XWT to the 11.5-m FODTS time series and the bay temperature (Figure 2c) and observe high XWT power at the 1-day and 0.5-day periods. Phase lag is not constant between the two time series indicating high coincident power but not correlation. The XWT between 30.5 m and bay temperature indicate high XWT power at the 1-day period (Figure 2c). The phase lag indicates that bay temperature precedes the FODTS temperature by 3.8 hours. Offshore, conduction of heat from the bay water and direct solar heating of the sediments are the dominating processes.

To infer the region of tidal pumping, we isolate and map CWT power at the 0.5-day period calculated for FODTS time series along the entire fiber-optic cable (Figs. 3a and 3c, respectively). The map of power for the tidal frequency clearly delineates a region of high power between about 7-13 m offshore, consistent with the zone of fresh groundwater discharge identified based on seepage measurements (Michael et al., 2003, 2005) (Figure 3a). During

intervals of low tidal range (e.g., JDs 172-174), the region of high semi-diurnal power appears to move landward. These results are consistent with XWT power between FODTS and tide stage (Figure 3b), which confirm high correlated power for the 0.5-day period. Based on the phase angle from XWT, a mean time lag of 3.4 hours was found between the tide stage and FODTS temperature in the zone of tidal pumping; hence discharge of cold groundwater lags the change in hydraulic gradient between the aquifer and the bay. We note that this time lag is dependent on the depth of the FODTS cable.

Following intense precipitation (e.g. one day prior to the start of the experiment and between JDs 186 and 188), correlated XWT power at the 0.5-day period extends out of the tidal pumping zone and over most of the FODTS transect (Figure 3b). The temperature response appears to lag these events by 3-4 days. This observation warrants additional investigation and is the focus of ongoing work but may indicate that discharge occurs along the whole transect following larger rain events, albeit at lower rates than in the tidal pumping zone, as indicated by relatively low power.

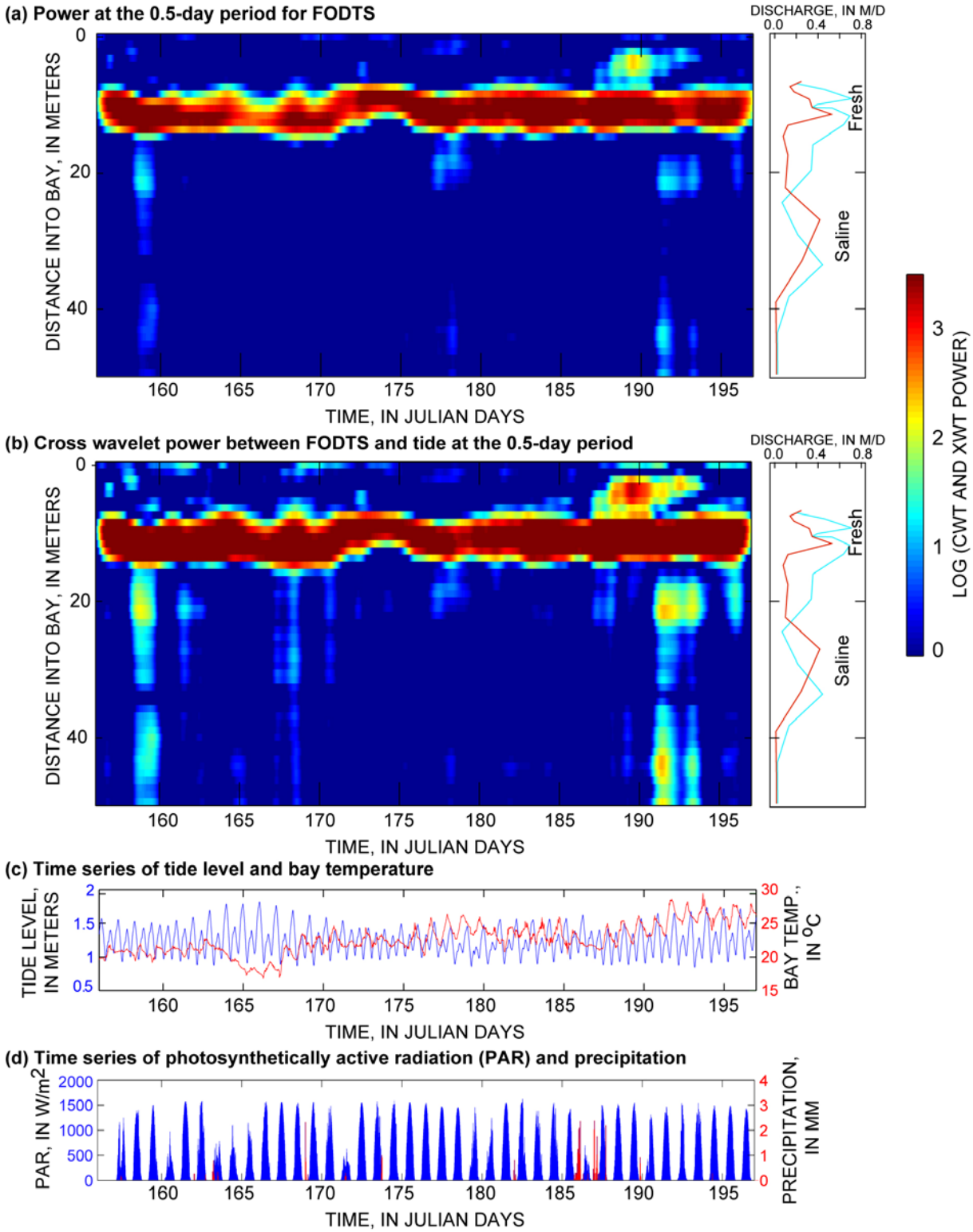

Figure 3. (a) Power at the semi-diurnal period for the FODTS as a function of location and time with measured discharge rates in meters per day (m/d) [after Michael et al., 2005]; (b) XWT power between FODTS and tide at the semi-diurnal period as a function of location and time with measured discharge rates [after Michael et al., 2005]; (c) time series of tide level (blue) and surface-water temperature (red); and (d) time series of photosynthetically active radiation (PAR) (blue) and precipitation (red).

5. Discussion and conclusions

FODTS can provide hydrologic insight at temporal and spatial scales that heretofore were difficult to investigate. Previous interpretation of FODTS data relied on simple time-series analysis based on variance (e.g., Lowry et al., 2007; Moffett et al., 2008). Here, we demonstrated the CWT and XWT for analysis of FODTS data from WBNERR, to isolate and map power at the tidal frequency and to investigate the effects of non-periodic forcing. The zone of tidal pumping of fresh SGD appears as a region of high CWT power at the tidal frequency; furthermore, this zone appears as a region of high power at the tidal frequency for the XWT calculated between FODTS data and tide stage. The XWT is a useful exploratory tool to identify relations between hydrologic forcing and aquifer response. Here, the XWT was applied to identify relations between subsurface and bay temperature, tides and precipitation.

Although we focused on the CWT and XWT, extension to other wavelet-based methods (e.g., wavelet transform coherence) is straightforward and the focus of ongoing work to identify relations between FODTS and other hydrologic time series. By identifying dominant modes of variability, correlations with mechanisms of influence, and non-stationary time lags between time series, wavelet methods provide powerful tools to explore large complex FODTS datasets and identify processes that control spatial and temporal patterns in temperature.

Acknowledgments

This work was supported by the U.S. Geological Survey Ground-Water Resources and Toxic Substances Hydrology Programs, NSF EAR 0548706, and the Singapore MIT Alliance for Research and Technology. The authors are grateful to Hanan Karam and Elena Abarca for field assistance; Matt Charette and Ann Mulligan for tide data; A. Grinsted, C. Torrence, and G.P. Compo for making their codes available; the WBNERR staff for field

support; and K. Singha, A. Pidlisecky and two anonymous reviewers for comments on the manuscript.

References

Anderson, M. P (2005), Heat as a Groundwater Tracer, *Ground Water*, *43*(6), 951-968.

Cambareri, T. C., and E. M. Eichner (1998), Watershed delineation and ground water discharge to a coastal embayment, *Ground Water*, *36*(4), 626–634.

Constantz, J., and D. A. Stonestrom (2003), Heat as a tracer of water movement near streams, *in* Stonestrom, D. A., and Constantz, J., eds., Heat as a tool for studying the movement of ground water near streams*, U.S. Geological Survey Circular 1260*, 1-63.

Grinsted, A., J. C. Moore, and S. Jevrejeva (2004), Application of the cross wavelet transform and wavelet coherence to geophysical time series, *Nonlinear Processes Geophys.*, *11*(5/6). 561-566.

Hatch, C. E., A. T. Fisher, J. S. Revenaugh, J. Constantz, and C. Ruehl (2006), Quantifying surface water - groundwater interactions using time series analysis of streambed thermal records: Methods development, *Water Resour. Res.*, *42*, W10410, doi: 10.1029/2005WR004787.

Kendall, A.D. and D.W. Hyndman (2007), Examining watershed processes using spectral analysis methods including the scaled-windowed fourier transform, in *Subsurface Hydrology Data Integration for Properties and Processes,* Hyndman, D.W., F. D. Day-Lewis, and K. Singha (eds.), AGU, Washington, DC, 183-200.

Kang, S., and H. Lin (2007), Wavelet analysis of hydrological and water quality signals in an agricultural watershed, *J. Hydrology*, *338*, 1-14.

Lowry, C. S., J. F. Walker, R. J. Hunt, and M. P. Anderson (2007), Identifying spatial variability of groundwater discharge in a wetland stream using a distributed temperature sensor. *Water Resour. Res.*, *43*, W10408, doi:10.1029/2007WR006145.

Michael, H. A., J. S. Lubetsky, and C. F. Harvey (2003), Characterizing submarine groundwater discharge: A seepage meter study in Waquoit Bay, Massachusetts, *Geophys. Res. Lett.*, *30*(6): doi:10.1029/2002GL016000.

Michael, H. A., A. E. Mulligan, and C. F. Harvey (2005), Seasonal oscillations in water exchange between aquifers and the coastal ocean, *Nature*, *436*, 1145-1148.

Moffett, K. B., S. W. Tyler, T. Torgerson, M. Menon, J. S. Selker, and S. M. Gorelick (2008), Processes controlling the thermal regime of saltmarsh channel beds, *ES&T*, *42*(3), 671–676.

Selker, J., L. Thevenaz, H. Huwald, A. Mallet, W. Luxumberg, N. van de Giesen, M. Stejskal, J. Zeman, M. Westhoff, and M. B. Parlange (2006), Distributed fiber-optic temperature sensing for hydrologic systems, *Water Resour. Res.*, *42*, W12202, doi. 10.1029/2006WR005326.

Taniguchi, M., J. V. Turner, and A. J. Smith (2003), Evaluations of groundwater discharge rates from subsurface temperature in Cockburn Sound, Western Australia, *Biogeochemistry*, *66*, 111-1243.

Torrence, C., and G. P. Compo (1998), A practical guide to wavelet analysis, *Bull. Am. Meteorol. Soc.*, *79*, 61-78.

Tyler, S.W., S.A. Burak, J.P. McNamara, A. Lamontagne, J.S. Selker, and J. Dozier (2008), Spatially distributed temperatures at the base of two mountain snowpacks measured with fiber-optic sensors, *J. of Glaciology, 54*(187), 673-679.